Integrated mode-evolution-based polarization splitter

M. R. Watts, H. A. Haus, and E. P. Ippen

Research Laboratory of Electronics, Massachusetts Institute of Technology, 77 Massachusetts Avenue, Cambridge, Massachusetts 02139

Received September 7, 2004

A mode-evolution-based polarization splitter suitable for high-index-contrast systems and directly integratable with a recently reported on-polarization rotator is described and its performance verified through both finite-difference time-domain and eigenmode expansion simulations. For a device length of 200 μm, greater than 22 dB of extinction is obtained across a 1.45–1.75-μm bandwidth. © 2005 Optical Society of America

OCIS codes: 130.2790, 130.3120, 230.5440.

High-index-contrast (HIC) dielectric waveguides exhibit highly confined optical modes. The tight confinement allows for waveguides to be spaced closely together without inducing cross talk and the propagating field to be guided around sharp bends with minimal radiative loss. However, as the index contrast is increased, the differences between the lateral boundary conditions for TE and TM modes become more pronounced, causing critical device parameters such as the propagation rate and the coupling strength to be polarization dependent. And, whereas the geometry of the waveguides may be designed to compensate for one or the other of these effects for a particular device, it is difficult to compensate for both simultaneously in a manner that applies to all devices on a HIC chip. To facilitate polarization-independent performance, a necessary feature for a standard single-mode-fiber-based communications link, one may circumvent the polarization sensitivity by implementing a polarization diversity scheme.[1,2] Such an approach requires the arbitrary polarization emanating from the fiber to be split into orthogonal components. By further rotating one of the outputs, one may achieve a single on-chip polarization, and the two paths may be operated on in parallel with identical structures. An integrated approach allows for the devices to be batch fabricated and the path lengths of the two arms to be matched through lithography.

Integrated polarization splitters come in two forms: 1, mode-coupling[3] and 2, mode-evolution-based devices.[4–9] Mode-coupling-based devices require phase-matched modes with precisely tuned coupling and are therefore inherently fabrication sensitive and wavelength dependent. Mode-evolution-based devices require only that mode coupling be suppressed, a looser requirement that permits more-relaxed tolerances and greater device bandwidths. Although many integrated optic polarization splitters have been proposed, with the exception of a device that was presented recently[9] they were not designed for the HIC systems in which they are most needed, nor have they been designed to interface with an integrated polarization rotator. Here we present an integrated polarization splitter designed for a HIC system that mates to a recently reported polarization rotator.[10]

The basic structure is depicted in Fig. 1. The input waveguide is a rectangular dielectric of horizontal orientation with width w_2 and height h. A vertically oriented guide of height $2h$ is formed at a separation s_1 from the horizontal guide, transitioned to a width w_1, and subsequently separated to a distance s_2. The initial separation s_1 avoids a point of intersection, which when fabricated would likely be nonadiabatic. The boundary condition imposed by Gauss's law causes modal confinement to be maximized for a polarization aligned along the geometric axis of the guide. A proper choice of h, w_1, and w_2 will ensure that the fundamental TE (i.e., TE_{11}) mode of the combined structure remains in the horizontally oriented guide while the fundamental TM (i.e., TM_{11}) mode transitions from the horizontally oriented guide to the vertically oriented guide. Although mode separation may be ensured, whether the power remains in the initially excited modes is a function of the degree of mode coupling induced by the evolving structure.

The coupling is described by coupled-local-mode theory.[11] Under weak coupling, coupling coefficient $\kappa(z)$,

$$\kappa(z) = \frac{\omega}{4\delta\beta(z)} \int_A \mathbf{e}_m^*(x,y,z) \cdot \mathbf{e}_n(x,y,z) \frac{\mathrm{d}}{\mathrm{d}z} \varepsilon(z) \mathrm{d}A, \tag{1}$$

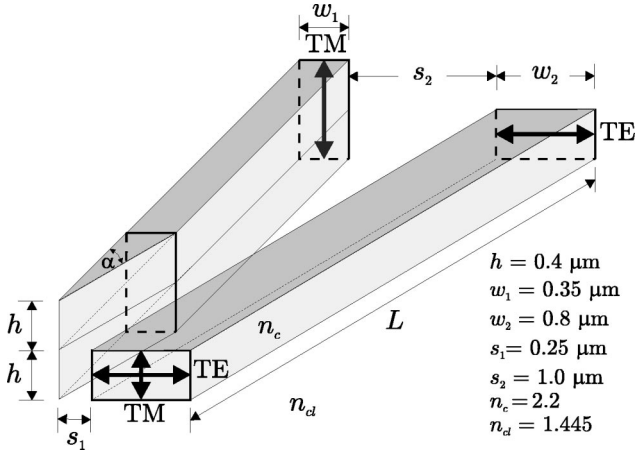

Fig. 1. Schematic of the polarization splitter.

0146-9592/05/090967-3/$15.00

where $\mathbf{e}_k(x,y,z)$ represents the normalized local vector electric field of mode k, may be replaced by its average, $\bar{\kappa}=(1/z)\int_0^z \kappa(z')\mathrm{d}z'$, and the power lost to a mode m is then determined to be[10]

$$P_m \propto 2\left|\frac{\bar{\kappa}}{\overline{\delta\beta}}\right|^2 [1-\cos(\overline{\delta\beta}z)], \tag{2}$$

where $\overline{\delta\beta}$ is the average difference in the rates of propagation between the modes. The larger the ratio of $\overline{\delta\beta}$ to $\bar{\kappa}$, the less power lost to a given mode. In HIC waveguides, unguided modes propagate at much higher rates than guided modes. Thus the two mode sets couple only through abrupt transitions. Coupling among guided modes is of greater concern because these modes propagate at similar rates. However, for strong coupling the modes must be similarly polarized. Although the input guide may be designed to propagate only the TE_{11} and TM_{11} modes, as the width of the vertically oriented guide is increased, secondary TE_{21} and TM_{21} modes develop. The power transfer is mitigated only by maintaining a large ratio of $\overline{\delta\beta}$ to $\bar{\kappa}$. One may always reduce the coupling [Eq. (1)] by reducing the rate of change in the dielectric (i.e., longer transitions), whereas $\overline{\delta\beta}$ is tied to the geometry of the guides. Large aspect-ratio guides help to ensure large values of $\overline{\delta\beta}$ for the like-polarized modes. Yet, for the TM modes that must exchange primary guides, $\overline{\delta\beta}$ is also intimately tied to initial separation s_1. Large initial separations lead to TM modes that approach degeneracy as the width of the vertically oriented guide is transitioned to w_1. And, whereas coupling between TE and TM modes is weak, a $\overline{\delta\beta}$ should be introduced to prevent it.

As an example, we chose guides with core indices of 2.2, cladding indices of 1.445, $h=0.4\ \mu$m, $w_1=0.35\ \mu$m, and $w_2=0.8\ \mu$m. The guides are rotated versions of one another, with a slight difference in the smaller dimension to break the degeneracy of the TE and TM modes. A chosen initial separation of $s_1=0.25\ \mu$m is large enough for fabrication but small enough for a large $\overline{\delta\beta}$ to be maintained between the TM modes. The modes at three cross sections of the example structure were calculated with a finite-difference mode solver for a wavelength of 1.55 μm. Figures 2 and 3 show the major field components of the TE and TM modes, respectively, and their effective indices $n_{\mathrm{eff}}=\beta\lambda/2\pi$ at various points along the transition. Figure 2 reveals that the TE_{11} mode remains in the horizontally oriented waveguide largely unaffected by the perturbation, whereas a TE_{21} mode develops in the vertically oriented guide. As only the TE_{11} and TM_{11} modes are initially excited, the fractional power in the TE_{21} and TM_{21} modes is determined by the power exchange induced by the transition. The TE modes exhibit little overlap in the region of perturbation and vastly different effective indices at all points along the transition. Thus, little power exchange is expected between the TE modes. However, from Figs. 3(a) and 3(b) we can see that the TM modes exchange guides. The transition, although it is necessary, causes the TM modes to exhibit much

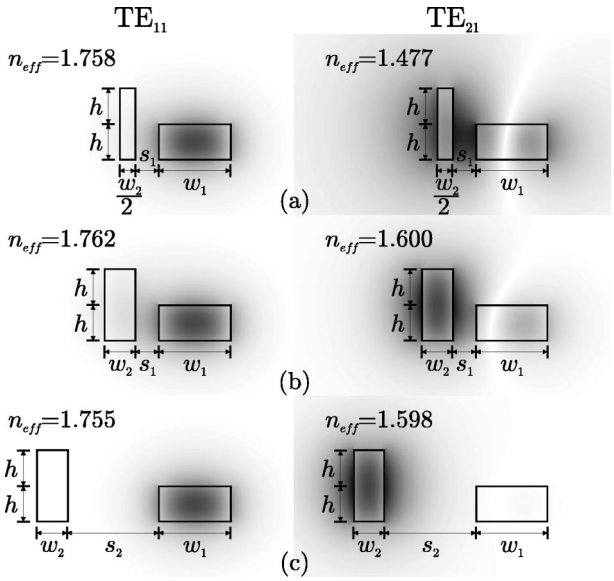

Fig. 2. Major electric field components of the (left) TE_{11} and (right) TE_{21} modes at three points along the transition. At a separation of $s_2=1.0\ \mu$m the TE_{11} mode clearly propagates in the horizontally oriented guide.

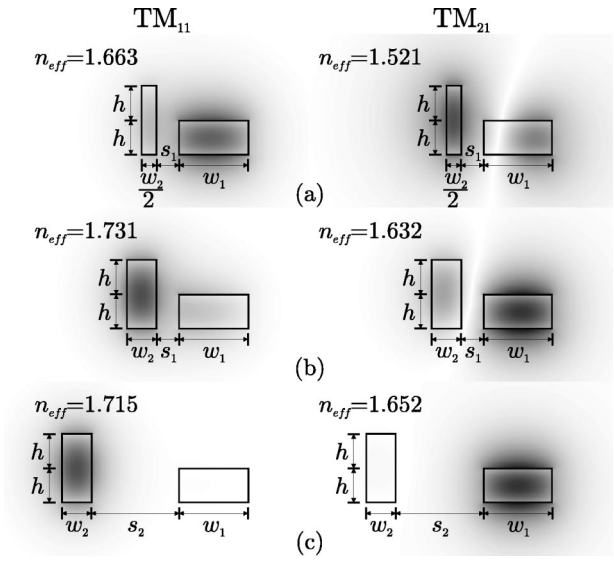

Fig. 3. Major electric field components of the (left) TM_{11} and (right) TM_{21} modes at three points along the transition. At a separation of $s_2=1.0\ \mu$m shown in (c) the TM_{11} mode clearly propagates in the vertically oriented guide.

greater overlap through the perturbation than their TE counterparts. Because the TM effective indices are also more similar, a power exchange among the TM modes is expected to limit the device's performance. Still, from Figs. 2(c) and 3(c) it is clear that, at a separation of $s_2=1\ \mu$m, the TE_{11} and TM_{11} modes propagate in separate guides. The modes have been isolated, and the waveguides may be rapidly separated.

To verify the approach, three-dimensional finite-difference-time-domain[12] (FDTD) and eigenmode-expansion[13] (EME) simulations were performed. We obtained FDTD results by separately launching TE

and TM input modes and monitoring the power in the TE and TM output modes. The primary guides were aligned to a uniform 25-nm FDTD grid to minimize spurious loss. The modal power was determined from the orthogonality relation for power normalized modes (i.e., $\delta_{mn}=\int \mathbf{e}_m\times\mathbf{h}_n\cdot\hat{\mathbf{z}}\mathrm{d}A$). EME results were obtained from the four guided modes. FDTD and EME results as functions of device length L at a wavelength of 1.55 μm are presented in Fig. 4(a). The lateral grid element for the 200-μm TM FDTD simulation was reduced to 12.5 nm to minimize grid-induced loss, yet Fig. 4(a) indicates that some spurious loss remains. Otherwise, the simulations are in agreement, confirming the intuition that coupling among guided TM modes limits performance. Slower transitions induce less coupling, allowing the modes a chance to dephase before they exchange substantial power. For lengths $L>200$ μm or angle $\alpha<0.0055$, the polarization splitting is nearly perfect. Spectral information obtained from a discrete Fourier transform in a FDTD simulation of a 200-μm-long device is presented in Fig. 4(b). More than 22 dB of extinction can be observed over the entire 1.45–1.75-μm regime.

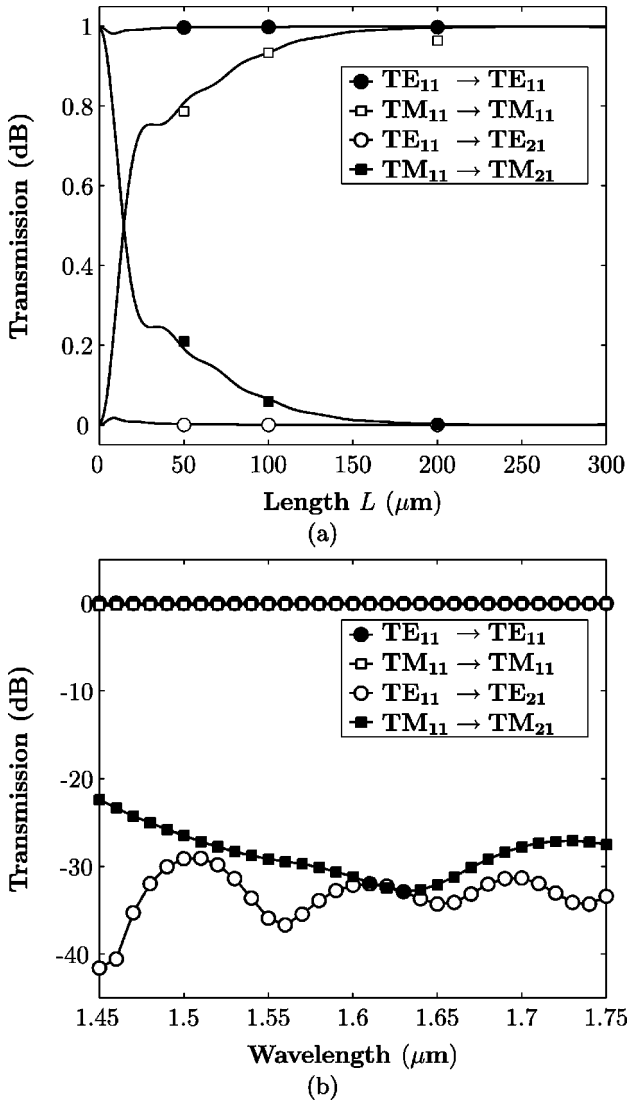

Fig. 4. (a) FDTD (points) and EME (solid curves) simulations as a function of device length and (b) FDTD-determined wavelength dependence for a 200-μm-long device.

It is important to note that features below 100 nm may not be obtained in fabrication. However, FDTD simulations indicate that a 100-nm blunt vertical guide tip induces only −38-dB $TE_{11}\rightarrow TE_{21}$ and −25-dB $TM_{11}\rightarrow TM_{21}$ cross talk along with −33-dB and −25-dB loss for the TE and TM cases, respectively, none of which significantly affects performance for device lengths $L\leqslant 200$ μm.

In summary, we have designed an integrated mode-evolution-based polarization splitter for a HIC system that mates to an existing polarization rotator to permit single on-chip polarization. The structure can be fabricated in only two lithographic steps, and a reasonable separation can be maintained between the TE and TM output guides at all points along the structure. FDTD and EME results confirm that near-perfect polarization splitting is achieved for device lengths greater than 200 μm. And, at a 200-μm length, greater than 22-dB extinction is achieved across the 1.45–1.75-μm band.

The authors are grateful to C. Manolatou for permitting the use of her FDTD code. This research was supported in part by Pirelli Labs and by U.S. Air Force Office of Scientific Research grant FA9550-04-1-0011. M. Watts's e-mail address is mwatts@mit.edu.

References

1. C. K. Madsen, Opt. Lett. **25**, 878 (2000).
2. M. R. Watts, "Wavelength switching and routing through evanescently induced absorption," M.S. thesis (Massachusetts Institute of Technology, Cambridge, Mass., 2001).
3. J. J. G. M. van der Tol, J. W. Pedersen, E. G. Metaal, J. J.-W. van Gaalen, Y. S. Oei, and F. H. Groen, IEEE Photonics Technol. Lett. **9**, 209 (1997).
4. N. Goto and G. L. Yip, J. Lightwave Technol. **7**, 1567 (1989).
5. Y. Shani, C. H. Henry, R. C. Kistler, K. J. Kazarinov, and R. F. Orlowsky, Appl. Phys. Lett. **56**, 120 (1990).
6. J. J. G. M. van der Tol and J. H. Laarhuis, J. Lightwave Technol. **9**, 879 (1991).
7. R. M. de Ridder, A. F. M. Sander, A. Driessen, and J. H. J. Fluitman, J. Lightwave Technol. **11**, 1806 (1993).
8. S. M. Garner, V. Chuyanov, S.-S. Lee, A. Chen, W. H. Steier, and L. R. Dalton, IEEE Photonics Technol. Lett. **11**, 842 (1999).
9. M. R. Watts, H. A. Haus, G. Gorni, and M. Cherchi, in *Integrated Photonics Research*, Vol. 91 of OSA Trends in Optics and Photonics Series (Optical Society of America, Washington, D.C., 2003), p. 26.
10. M. R. Watts and H. A. Haus, Opt. Lett. **30**, 138 (2005).
11. A. W. Snyder, *Optical Waveguide Theory* (Chapman & Hall, London, 1983), pp. 553–557.
12. A. Taflove, *Computational Electromagnetics: the Finite-Difference Time-Domain Method* (Artech House, Norwood, Mass., 1995).
13. FIMMPROP software by Photon Design, Oxford, UK.